

Minocycline Immunomodulates via Sonic Hedgehog Signaling and Apoptosis and Has Direct Potency Against Drug-Resistant Tuberculosis

Devyani Deshpande,¹ Jotam G. Pasipanodya,¹ Shashikant Srivastava,¹ Katherine R. Martin,¹ Shruti Athale,¹ Johanna van Zyl,¹ John Antiabong,¹ Thearith Koeuth,¹ Pooi S. Lee,¹ Keertan Dheda,² and Tawanda Gumbo^{1,2}

¹Center for Infectious Diseases Research and Experimental Therapeutics, Baylor Research Institute, Dallas, Texas; and ²Division of Pulmonology, Centre for Lung Infection and Immunity, University of Cape Town Lung Institute, South Africa

Drug-resistant tuberculosis represents a global emergency, requiring new drugs. We found that minocycline was highly potent in laboratory strains of *Mycobacterium tuberculosis* and that 30 drug-susceptible and multidrug/extensively drug-resistant clinical strains were susceptible to clinically achievable concentrations. In the hollow fiber system model, lung concentration-time profiles of 7 mg/kg/day human-equivalent minocycline dose achieved bacterial kill rates equivalent to those of first-line antituberculosis agents. Minocycline killed extracellular bacilli directly. Minocycline also killed intracellular bacilli indirectly, via concentration-dependent granzyme A-driven apoptosis. Moreover, minocycline demonstrated dose-dependent antiinflammatory activity and downregulation of extracellular matrix-based remodeling pathways and, thus, could protect patients from tuberculosis immunopathology. In RNA sequencing of repetitive samples from the hollow fiber system and in independent protein abundance experiments, minocycline demonstrated dose-dependent inhibition of sonic hedgehog-patched-gli signaling. These findings have implications for improved lung remodeling and for dual immunomodulation and direct microbial kill-based treatment shortening regimens for drug-susceptible and drug-resistant latent and active *M. tuberculosis* infection.

Keywords. Smac/DIABLO; caspase 3; PTCH1; GLI1; lung remodeling; host-directed therapy.

Tuberculosis is arguably the most important infectious killer of mankind. Until the advent of chemotherapy in the 1940s, outcomes were hopeless. Around that time, Duggar discovered tetracyclines [1]. Given the desperate situation, Wolinsky and Steenken examined the efficacy of oxytetracycline and chlortetracycline efficacy against tuberculosis, but these first-generation tetracyclines had limited efficacy and considerable toxicity [2, 3]. Tetracyclines further fell out of favor for tuberculosis treatment after the discovery of safer and efficacious first-line drugs. By 1964, Pines noted that even when 4–5 g of tetracycline were given daily in combination with first-line drugs, they observed universally poor activity and opined that “tetracycline has very little place in the treatment of tuberculosis” (page 311) [4]. In the meantime, the second-generation tetracyclines doxycycline and minocycline were patented in 1957 and 1961, respectively [5]. It has been hypothesized that doxycycline could be a potential adjunctive therapy for multidrug-resistant tuberculosis (MDR-TB) by reducing *Mycobacterium tuberculosis*-associated

immunopathological damage, via inhibition of matrix metalloproteinase (MMPs); however, doxycycline minimum inhibitory concentrations (MIC) for *M. tuberculosis* were high [6–8]. However, because of the emergence of MDR-TB and extensively drug-resistant tuberculosis (XDR-TB), we are once more as desperate as in the prechemotherapy era for treatments that can be used in these patient groups [9, 10]. As a result, we recently designed a rapid translation program to examine the effect of all antibiotic pharmacophores on *M. tuberculosis*: ceftazidime-avibactam and benzylpenicillin were the first hits [11, 12]. Here, we examined minocycline through the same program.

Minocycline has several characteristics that could make it attractive for the treatment of tuberculosis. First, it has an oral bioavailability of approximately 100%, with a serum peak concentration of 3.5 mg/L on standard dosing [13]. Second, minocycline's tissue-to-serum concentration ratio is 3.8 for lung parenchyma [13–15]. Third, its long serum half-life of 12–18 hours could allow the design of intermittent regimens [13]. Fourth, minocycline was well tolerated when up to 10 mg/kg (maximum, 700 mg) was given intravenously each day, with a maximum serum peak concentration of 25 mg/L [16, 17]. Fifth, minocycline has clinically proven antiinflammatory activity for conditions such multiple sclerosis via inhibition of MMPs and nuclear factor of activated T-cell (NFAT)-mediated transcriptional activation that attenuates CD4⁺ T-cell activation [18, 19]. It is neuroprotective after cerebrovascular accidents and viral encephalitides, which could

Received 11 June 2018; editorial decision 24 September 2018; accepted 14 November 2018; published online December 28, 2018.

Correspondence: Tawanda Gumbo (tawanda.gumbo@BSWHealth.org).

The Journal of Infectious Diseases® 2019;219:975–85

© The Author(s) 2018. Published by Oxford University Press for the Infectious Diseases Society of America. All rights reserved. For permissions, e-mail: journals.permissions@oup.com. DOI: 10.1093/infdis/jiy587

be important in reducing the severe postneurological sequelae in patients with tuberculous meningitis [16, 20]. Sixth, minocycline has proven efficacy against another slow-growing mycobacterium, *Mycobacterium leprae*, for which it is safely administered daily for 24 months. Here, we tested for minocycline efficacy in our hollow fiber system model of tuberculosis (HFS-TB), which has a forecasting accuracy of >94% in predicting clinical outcomes and optimal antituberculosis doses, has been qualified as a drug-discovery tool by the European Medicine Agency, and is endorsed by the US Food and Drug Administration [21–23].

MATERIALS AND METHODS

Bacterial Strains, Cell Lines, and Materials

The *M. tuberculosis* laboratory strains used in the experiments were H37Ra (ATCC catalog no. 25177), H37Rv (ATCC catalog no. 27294), CDC1551, and HN878. Twenty-five clinical *M. tuberculosis* strains collected by the Medical Research Council in South Africa and 5 from National Jewish Health in Colorado (donated by Dr Max Salfinger) were also used for MIC testing. Hollow fiber cartridges were purchased from FiberCell (Fredrick, MD). Minocycline, cyclopamine, and staurosporine were purchased from Sigma-Aldrich (St. Louis, MO).

Determination of Minocycline Activity and MICs

First, we examined the effect of minocycline extracellularly, in test tubes, on *M. tuberculosis* H37Ra in the log phase of growth and intracellularly in *M. tuberculosis* H37Ra–infected human-derived THP-1 cell–adherent macrophages in 12-well plates, as described elsewhere [12]. THP-1 cells (ATCC TIB -202), grown in Roswell Park Memorial Institute 1640 medium plus 10% fetal bovine serum (RPMI/FBS), were infected with log-phase *M. tuberculosis* H37Ra at a multiplicity of infection of 1:1 [24, 25]. Minocycline MICs were identified using broth macrodilution and mycobacterial growth indicator tube kits [12, 24]. The final minocycline concentrations coincubated with the *M. tuberculosis* strains were 0, 0.125, 0.25, 0.5, 1, 2, 4, 8, and 16 mg/L. All isolates were examined in duplicate. Each experiment was performed twice.

The HFS-TB Model

The HFS-TB model, described in detail elsewhere, allows us to test the effect of human lung–like drug concentration–time profiles [11, 12, 24–27]. In brief, 20 mL of *M. tuberculosis*–infected THP-1 cells were inoculated into peripheral compartments of HFS-TB preconditioned for 72 hours with RPMI/FBS. Minocycline was infused via computer-programmed syringe pumps over 1 hour. We mimicked the half-life of 12 hours and a lung penetration ratio of 3.8:1 in all HFS-TB units [13–15]. The bacterial burden at indicated time points was determined by measuring the number of colony-forming unit (CFU) on Middlebrook 7H10 agar supplemented with 10% oleic albumin dextrose catalase and by measuring the time to positive results of the mycobacterial growth indicator tube assay. A detailed description of the assays

for measurement of extracellular and intracellular minocycline concentrations is in the Supplementary Methods.

RNA Sequencing and Analysis

RNA extraction and sequencing of HFS-TB contents was performed using methods described elsewhere [24, 26]. We realigned the sequences to the HumanRefSeqBuilt37 (GRCh37p13), using CLC Genomic Workbench software, version 8. Differentially expressed genes (DEGs) were defined by comparing minocycline-treated HFS-TB reads to the non-treated reads on the same sampling day, based on a Bonferroni adjusted *P* value of <.05. Pathway analysis of DEGs was performed using Ingenuity Pathway Analysis.

Apoptosis and Sonic Hedgehog (SHH) Signaling Studies in 12-Well Plates

Noninfected adherent THP-1 cells in 12-well plates were exposed to different minocycline concentrations or to cyclopamine (a known inhibitor of SHH) or to staurosporine (which induces caspase 3 [CASP3]–dependent apoptosis). Supernatant was collected repeatedly over 28 days to measure concentrations of SHH proteins, the receptor protein patched homolog 1 (PTCH1), whose binding relieves inhibition of the protein smoothed (SMO), which enters the cytoplasm to activate the transcriptional factor glioma-associated oncogene 1 (GLI1), using an enzyme-linked immunosorbent assay. PTCH1 and CASP3 concentrations were measured from cell lysate. Further details of the assays are given in the Supplementary Methods.

Apoptosis Study in the HFS-TB

To determine whether this minocycline-induced apoptosis led to *M. tuberculosis* killing, we performed a separate intracellular *M. tuberculosis* HFS-TB study. The systems were treated with once daily minocycline doses (half-life, 12 hours) that achieved peak concentrations of 0, 0.25, 0.5, 1, and 10 times the MIC for 26 days. Sampling details are in the Supplementary Methods.

Statistical and Pharmacokinetic/Pharmacodynamic Analyses

Compartmental pharmacokinetic modeling of drug concentrations was performed as described previously [11, 12, 28]. Pharmacodynamic relationships, such as the minocycline 0–24-hour area under the concentration–time curve (AUC_{0-24}) versus the *M. tuberculosis* burden (both the time to positivity and the number of CFU per milliliter) or versus the number of RNA sequence reads per kilobase of transcript per million mapped reads (RPKM), were examined using the inhibitory sigmoid maximal effect model, which has the following 4 parameters: maximal kill (E_{max} ; calculated as the number of CFU per milliliter, the time to positivity, or the RPKM), concentration or exposure associated with 50% of maximal kill (EC_{50}), Hill factor, and effect in non-treated controls [12, 28, 29]. For protein concentration studies, Student *t* tests and analysis of variance (ANOVA) for repeated measures were performed to determine the difference between groups, as described in detail in the Supplementary Methods.

Monte Carlo Experiments

We used the pharmacokinetics of minocycline from patients in the MINOS study and those from the study by Yamamoto et al in Monte Carlo experiments [16, 30]. The pharmacokinetic parameter estimates and variability used are shown in [Supplementary Table 1](#). We examined for the achievement of exposure associated with 80% of E_{\max} (EC_{80}) exposures in lungs of 10 000 patients with pulmonary tuberculosis treated with 2, 3, 4, 5, 6, and 7 mg/kg orally daily, following steps further described in detail in the Supplementary Methods. The MIC distribution used in the simulations was that obtained from our 30 clinical isolates.

RESULTS

Effect of Minocycline Exposure on *M. tuberculosis* in Test Tubes and 12-Well Plates and on MDR-TB/XDR-TB

In test tubes with extracellular *M. tuberculosis* in the log phase of growth, the mean minocycline E_{\max} (\pm SD) was $5.79 \pm 0.29 \log_{10}$

CFU/mL, with a mean EC_{50} (\pm SD) of 0.35 ± 0.05 mg/L ($r^2 = 0.96$; [Figure 1A](#)). The E_{\max} exceeds that of the first-line drugs isoniazid and pyrazinamide and equals that of rifampin in the same assay [12]. In 12-well plates of intracellular *M. tuberculosis*, the mean minocycline E_{\max} (\pm SD) was $3.57 \pm 0 \log_{10}$ CFU/mL, and the mean EC_{50} (\pm SD) was 0.95 ± 0.25 mg/L ($r^2 = 0.97$; [Figure 1B](#)). Thus, the EC_{50} is multiple times lower than minocycline's lung peak concentration achieved by the standard daily dose of 200 mg.

The MICs in 4 standard virulent laboratory strains are shown in [Figure 1C](#). The MICs of 30 clinical isolates (of which 81% were either MDR or XDR) are shown in [Figure 1D](#). A total of 94% of isolates had MICs below clinically achievable minocycline concentrations in lung tissue.

Minocycline Concentrations in the HFS-TB and Intracellularly Infected Monocytes

The minocycline concentration-time profiles achieved in the extracellular compartment of each HFS-TB, based on

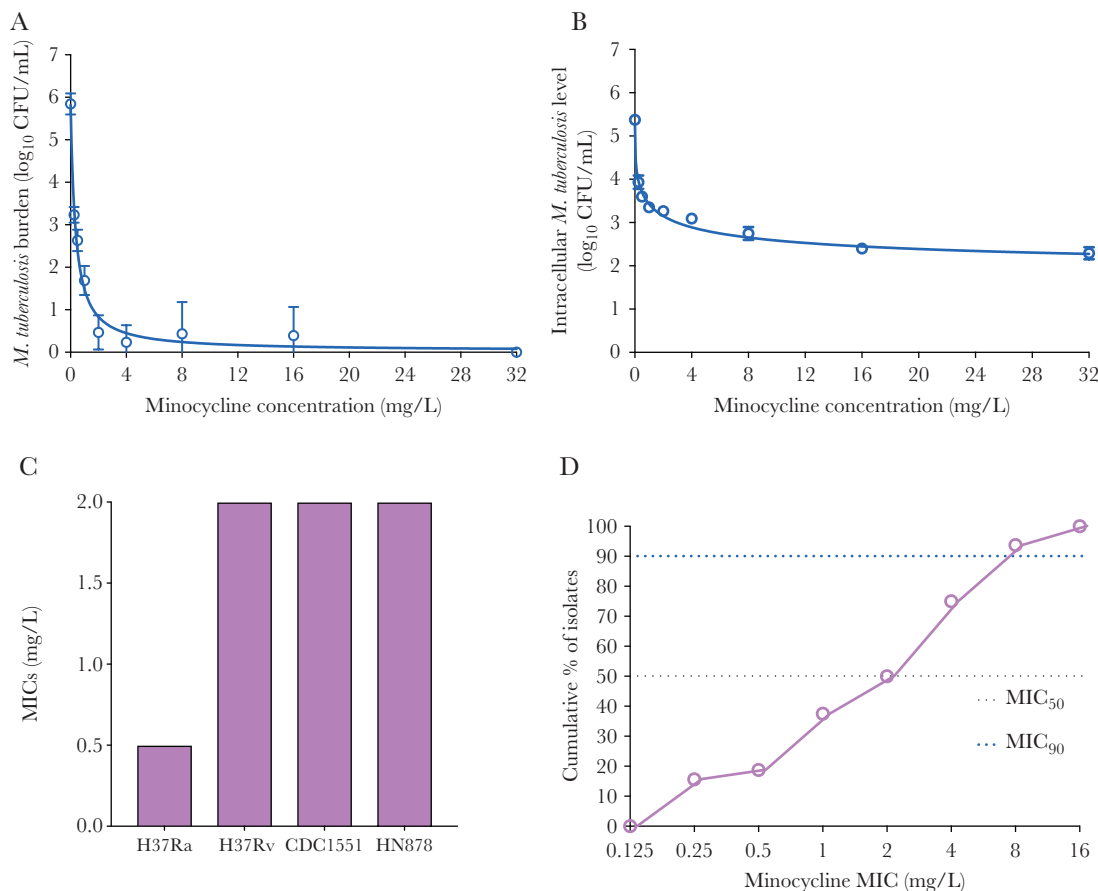


Figure 1. Effect of the minocycline concentration on *Mycobacterium tuberculosis*. Each minocycline concentration was examined in triplicate. Circles denote mean values, and whiskers denote standard deviations. The effect of concentration on \log_{10} number of colony-forming units (CFU) per milliliter was modeled using the inhibitory sigmoid maximal kill curve for both the extracellular and intracellular studies. **A**, Minocycline wiped out log-phase *M. tuberculosis* completely in 7 days in this assay. **B**, Minocycline's efficacy against intracellular *M. tuberculosis* was only slightly less than that against log-phase *M. tuberculosis*. **C**, Minimum inhibitory concentrations (MICs) determined by the mycobacterial growth indicator tube kit (Bactec) are shown for 4 laboratory strains; the MIC was ≤ 2 mg/L. **D**, Cumulative responses of 30 clinical isolates from South Africa and the United States show that, for all clinical isolates examined, including those with higher MICs, the MICs remained below clinically achievable concentrations in the lung, given that minocycline is concentrated in the lungs for most isolates.

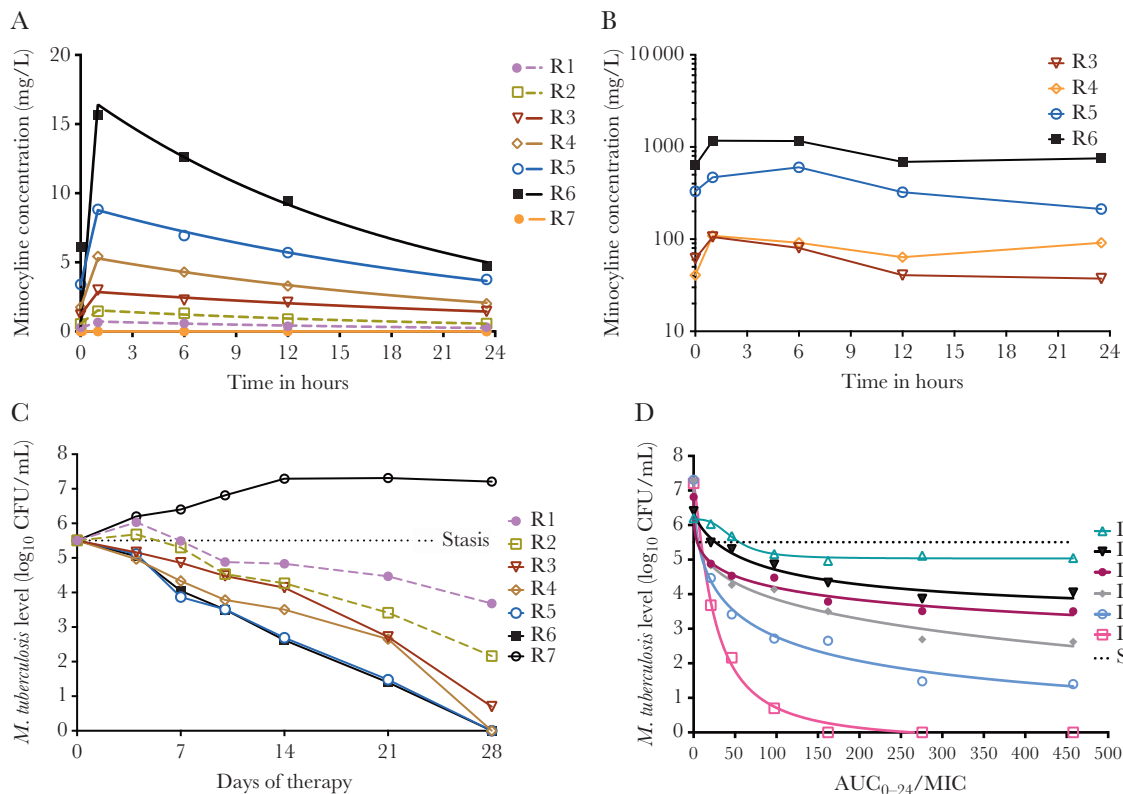


Figure 2. Efficacy of minocycline in the hollow fiber system model of tuberculosis. Minocycline, administered on a once daily schedule to mimic human concentration-time profiles in patients, was administered at 6 different doses, numbered R1 to R6, with R7 denoting no treatment. We measured drug concentrations 10 minutes prior to the last dose on day 28 and then at 1, 6, 12, and 24.5 hours. *A*, Concentration-effect in extracellular fluid revealed a mean elimination rate constant (\pm SD) of 0.046 ± 0.008 per hour, shown by the line graphs, which translates to a mean half-life (\pm SD) of 16.00 ± 3.2 hours. To put this into context, the average steady-state 24-hour area under the concentration-time curve (AUC_{0-24}) achieved by the standard 200-mg oral dose of minocycline in serum is 44–48 $\text{mg} \cdot \text{h}/\text{L}$ and thus, in the lung tissue (3.8-fold), would be equivalent to the R5 dose in panel *A*. *B*, Inside infected monocytes, concentrations were several times greater, such that we resorted to a \log_{10} scale on the y -axis. The shape also differed from that in panel *A*. *C*, Based on the number of colony-forming units (CFU) per milliliter, several doses would be considered to have completely sterilized the systems by the end of week 4. *D*, The model fits using the \log_{10} number of CFU per milliliter were even better, with an r^2 ranging from 0.97 to >0.99 .

measured concentrations, are shown in [Figure 2A](#). The minocycline concentration-time profiles achieved in infected monocytes by doses R3–R6 are also shown in [Figure 2B](#). The shape of the intracellular concentration-time curve differed dramatically from the extracellular concentrations in these HFS-TB and was consistent with hysteresis (see Discussion). The mean intracellular to extracellular AUC_{0-24} ratios (\pm SD) were 52 ± 32 . This means that intracellular *M. tuberculosis* will be exposed to concentrations above the MIC for virtually all clinical isolates in [Figure 1D](#).

There was a dose-dependent decrease in bacterial burden throughout treatment, whereas the bacterial burden increased without treatment ([Figure 2C](#) and [Supplementary Figure 1A](#)). Results of the inhibitory sigmoid E_{\max} model of the minocycline AUC_{0-24} to MIC ratio versus the *M. tuberculosis* burden are shown in [Figure 2D](#) (for the number of CFU per milliliter) and [Supplementary Figure 1B](#) (for the time to positivity). Based on this, the EC_{80} on day 28 had an AUC to MIC ratio of 71.58.

Minocycline RNA Sequencing Signature From Serial Sampling of Each HFS-TB

RNA sequencing of infected monocytes repetitively and sequentially sampled from each HFS-TB had good quality scores ([Supplementary Figure 2](#)). The number of DEGs ([Figure 3A](#) and [3B](#)) demonstrated that, by 28, minocycline resulted in higher numbers of downregulated genes than upregulated ones; all significant DEGs are shown in [Supplementary Table 2](#). Ingenuity Pathway Analysis of the DEGs revealed that they mapped to pathways shown in [Supplementary Table 3](#). We ranked the top 20 most extensively regulated pathways according to the fold changes in their expression ([Figure 3C](#)). For context and as a positive control, [Figure 3C](#) also shows the downregulation of NFAT expression, which was validated by others as being downregulated by minocycline [19]. The pathways that were most upregulated and downregulated were consistent with (1) granzyme A (GZMA) signaling-based apoptosis, (2) predominantly downregulated inflammatory signaling pathways, and (3) extracellular matrix (ECM) signaling related pathways (ephrin

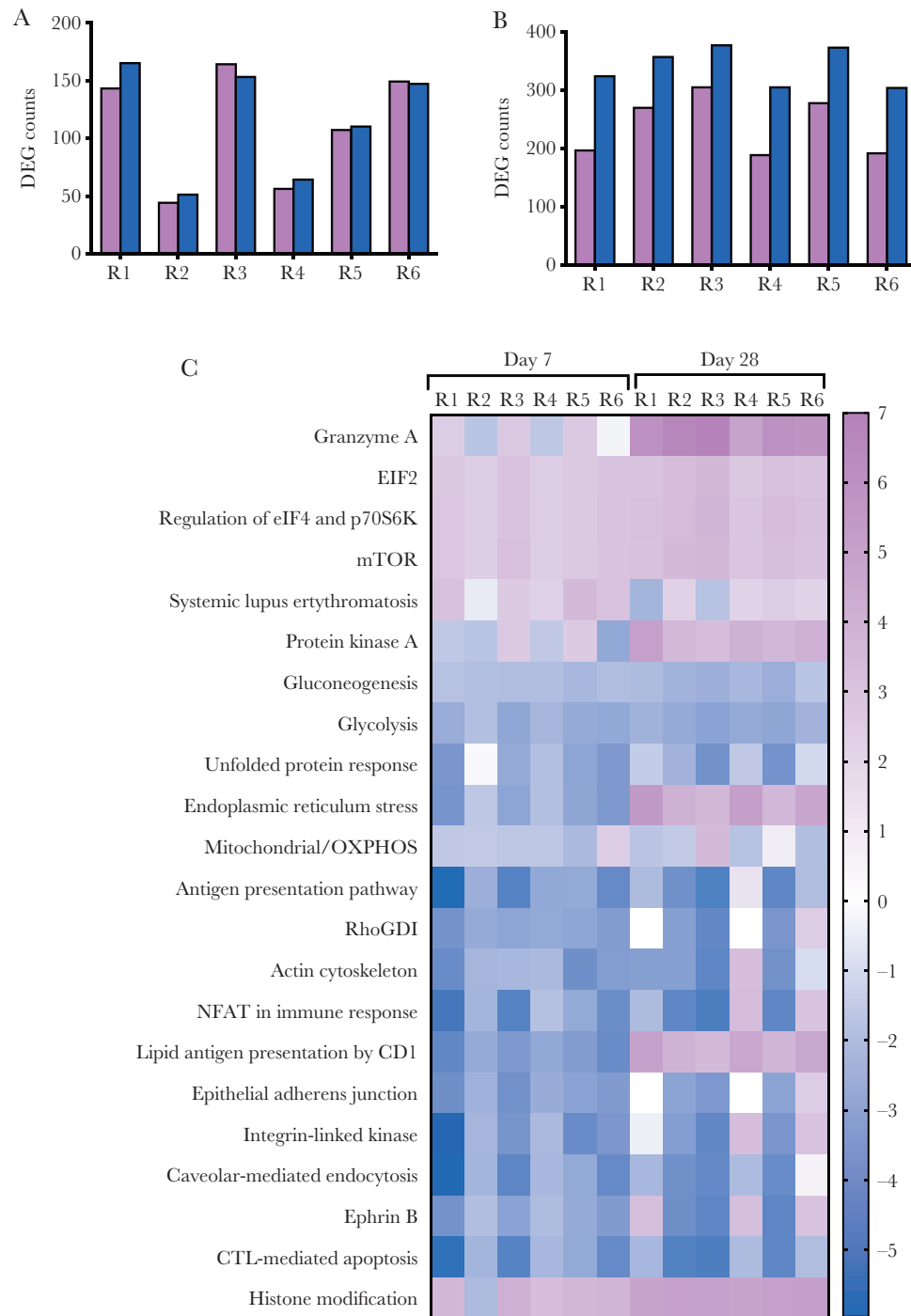


Figure 3. RNA sequencing to determine signaling pathways based on different minocycline doses. Hollow fiber system model of tuberculosis (HFS-TB) replicates were treated once daily with minocycline doses exhibiting 0–24-hour area under the concentration-time curve (AUC_{0-24}) values of 10.5 mg*h/L (R1), 22.8 mg*h/L (R2), 48.5 mg*h/L (R3), 80.9 mg*h/L (R4), 137.6 mg*h/L (R5), and 224.6 mg*h/L (R6) or were untreated and were sampled on days 7 and 28 for RNA sequencing analysis. Differentially expressed genes (DEGs) and fold change in expression were determined relative to values for no treatment and are shown in [Supplementary Table 2](#). *A*, Findings on day 7 revealed a balance between the number of upregulated and downregulated genes. *B*, By 28, the number of DEGs had increased, and more were downregulated. *C*, Fold changes in the regulation of pathways (and not individual DEGs) are shown on the scale bar on the right on a magenta (upregulated) to blue (downregulated) scale. The most upregulated gene was *GZMA*. Although histone genes were overexpressed, examination of each histone posttranscriptional modification gene revealed that none were significantly differentially expressed. One of the surprise findings was upregulation of the systemic lupus erythematosis pathway, attesting to the advantages of unbiased genome-wide analyses. Minocycline-induced lupus is a rare but well described clinical entity, and our results mean that RNA sequencing of HFS-TB cell line contents was sensitive enough to identify this rare clinical entity and reveal the signature of an otherwise systemic inflammatory condition. CTL, cytotoxic T lymphocyte.

B, actin cytoskeleton, RhoGD1, and integrin-linked kinase) and remodeling of epithelial adherens junctions (Figure 3C).

Minocycline-Based Apoptosis Assays in 12-Well Plates and the HFS-TB

The most upregulated pathway in Figure 3C was GZMA signaling, especially on day 28. The first intracellular action of GZMA is interference with mitochondrial electron transport chain/oxidative phosphorylation and disruption of the mitochondrial membrane potential, which was downregulated (Figure 3C); this leads to apoptosis via the intrinsic pathway [31]. In addition, paradoxically, one of the most downregulated pathways was cytotoxic T-cell-mediated apoptosis (Figure 3C). There was no gene for which expression was significantly differentially expressed in the entire Fas ligand pathway and the TNF pathways, with the exception of *MCL1*, which encodes for one of the most potent antiapoptotic factors in the Bcl-2 family, which was downregulated on day 7 (Supplementary Figure 3).

In 12-well plates, the effects of staurosporine and several concentrations of minocycline on CASP3 concentration were determined (Figure 4). Minocycline concentrations demonstrated changes in the same direction as those of the positive control, staurosporine (Figure 4A); CASP3 activation (normally under inhibition by inhibitor of apoptosis [IAP] protein) is crucial for execution of both intrinsic and extrinsic apoptosis pathways. ANOVA demonstrated that the effect of minocycline on CASP3 was time dependent (Figure 4B). Moreover, there was a minocycline versus CASP3 concentration dose response for each sampling day (Figure 4C).

HFS-TB results of minocycline-induced apoptosis are shown in Figure 5A and 5B, with sub-MIC peak concentrations killing intracellular *M. tuberculosis*. In addition, on day 21, Western blot densitometry of direct IAP binding protein with a low pI (DIABLO) of HFS-TB contents demonstrated a significantly higher DIABLO concentration in HFS-TB units treated with doses achieving sub-MIC doses, compared with the nontreated HFS-TB replicates (Figure 5C). Overall, Figure 5 shows microbial kill by sub-MIC doses, higher DIABLO, and higher CASP3 concentrations, while RNA sequences demonstrated GZMA pathway upregulation, consistent with a minocycline concentration-dependent increase in apoptosis.

Discovery of Minocycline's Effect on SHH Signaling

RNA sequencing by Ingenuity Pathway Analysis also demonstrated ECM signaling-related pathways as being among the most downregulated, suggesting an effect on pathways related to lung remodeling (Figure 3). We detected a 10-fold increase in *TIMP1* expression at day 28 as compared to day 7 in minocycline-treated HFS-TB, in parallel with a similar decreases in the magnitudes of *MMP2*, *COL1A*, and *COL9A2* expression (Supplementary Figure 4). Thus, minocycline affected *TIMP1* and *MMP2* transcription, as has been hypothesized for doxycycline. The most downregulated of all ECM DEGs was *COL9A2*, followed by *COL1A1* (Supplementary Figure 4). *COL9A2* has

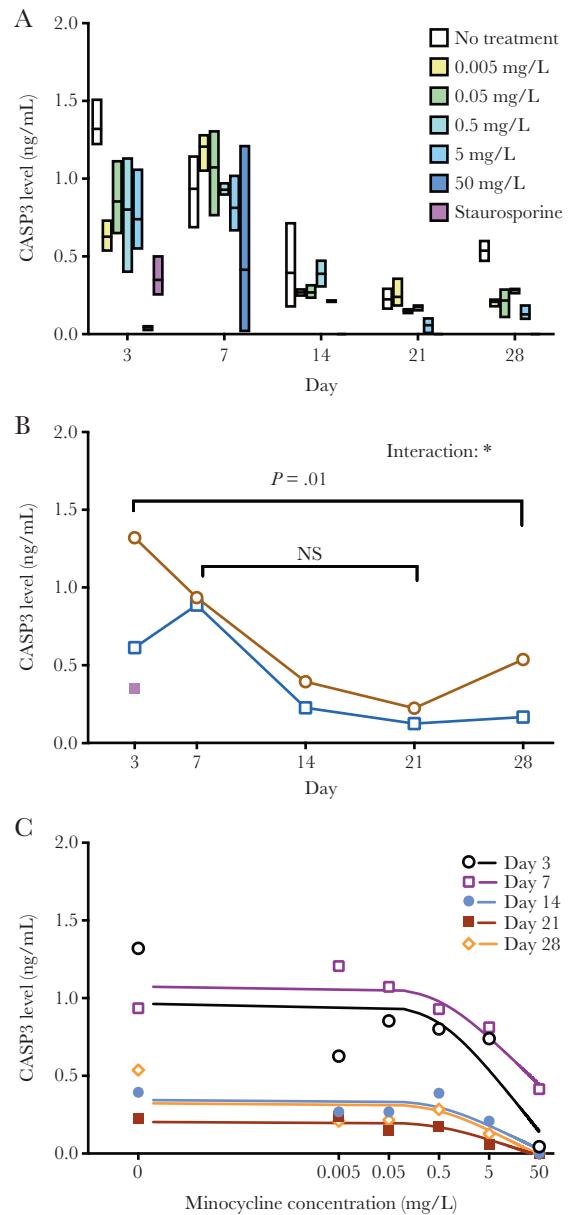


Figure 4. Effect of minocycline on the apoptosis protein caspase 3 (CASP3) in 12-well plates. The effect of staurosporine (a positive control that induces apoptosis) and different minocycline concentrations on CASP3 is shown for triplicate wells for each. *A*, Mean, minimum, and maximum CASP3 concentrations at each time point. Staurosporine results are available only for day 3, since the drug killed THP-1 cells after that point; minocycline results were similar to those for staurosporine (ie, minocycline was associated with decreased CASP3 levels over time). On day 3, 50 mg/L minocycline was more effective than staurosporine. *B*, When we combined the different concentrations of minocycline and compared them to no treatment or staurosporine by use of repeated measures analysis of variance (ANOVA), we identified a significant interaction between time and treatment group ($P = .0272$). Therefore, we performed 2 secondary ANOVAs between days 3 and 28 and between days 7 and 21. Minocycline treatment significantly decreased CASP3 levels, compared with no treatment ($P = .0011$), on days 3 and 28, but differences were not significant between days 7 and 21 ($P = .086$). Staurosporine treatment yielded significantly reduced CASP3 concentrations, compared with no treatment ($P = .0019$) but not compared with minocycline treatment ($P = .0614$). *C*, Using a quantitative pharmacologic approach, minocycline had a dose-response effect on the CASP3 level, with the steep portion of the dose-response curve in the clinically achievable concentration range of 0.5 to 5 mg/L (r^2 range, 0.75 at day 28 to 0.94 at day 7). NS, not significant.

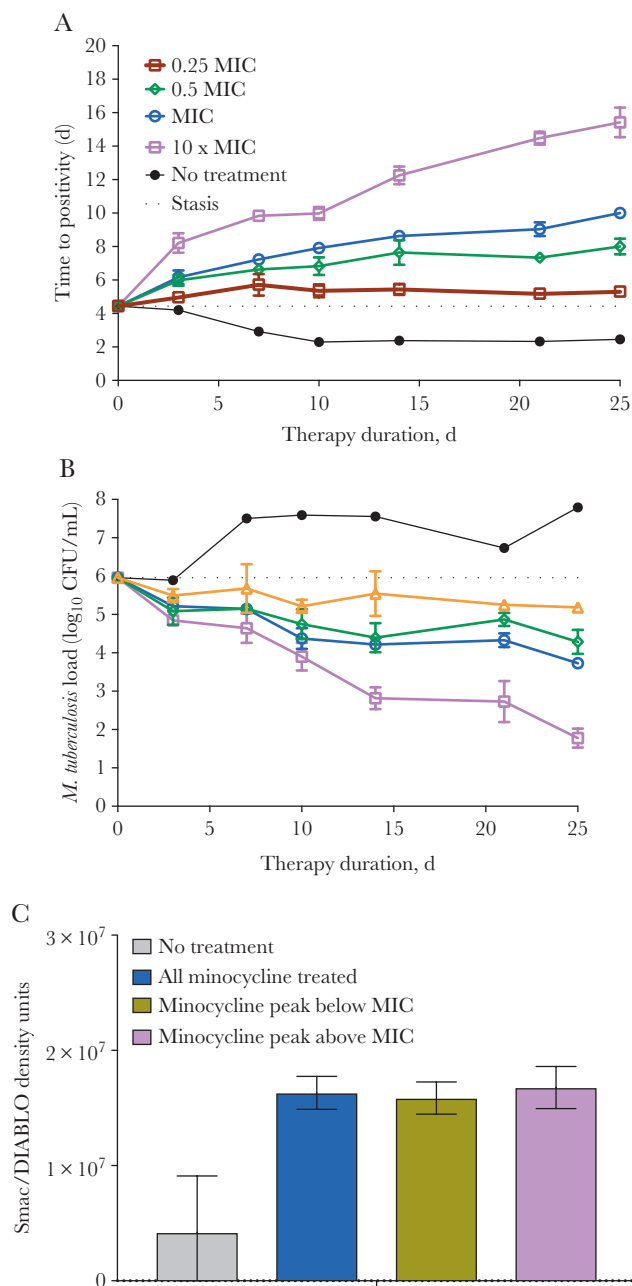


Figure 5. Minocycline-induced apoptosis and killing of intracellular bacilli in the hollow fiber system model of tuberculosis (HFS-TB). *A*, HFS-TB study involving intracellular *Mycobacterium tuberculosis* with 2 replicate units treated with minocycline doses that declined with a half-life of 12 hours but achieved the peak concentrations shown. The time to positivity decreased as the bacterial burden increased; even the dose associated with 0.25 times the minimum inhibitory concentration (MIC) resulted in a time to positivity longer than at the start of experiment, demonstrating microbial kill. *B*, Similar results are shown when the number of colony-forming units per milliliter was used as a readout. *C*, Densitometry results of a Western blot for direct inhibitor of apoptosis protein with low pI (DIABLO) in the same HFS-TB system treated with minocycline that killed *M. tuberculosis*; results are from day 21 of treatment. DIABLO neutralized inhibitors of apoptosis inhibitory proteins to release caspase 3 and activate it so that apoptosis occurs. The minocycline-treated HFS-TB systems yielded higher concentrations of DIABLO than no treatment, which resulted in higher rates of apoptosis.

been associated with fibrosis in cartilage matrix in bones and joints, whereas upregulation of *COL1A1* is a part of the fibrotic lung response, is part of the tuberculous lung response, and is associated with increased matrix stiffening [32–34].

Comparison of RPKM values in minocycline-treated versus nontreated HFS-TB contents for genes encoding proteins in pathways known to influence lung remodeling, such as transforming growth factor β (TGF- β), NOTCH, CAV-1, WNT, and SHH signaling [35–39], was performed (Supplementary Figure 5). The Student *t* test revealed that expression of only the genes for SHH and the related WNT signaling pathway were significantly different (Supplementary Figure 5). When the minocycline AUC_{0–24} versus the RPKM sum of all the genes in each of these pathways (response) was examined using the inhibitory sigmoid E_{max} model, convergence was achieved for SHH signaling ($r^2 = 0.65$; Supplementary Figure 5B) but not for WNT signaling. Therefore, we evaluated the minocycline dose-dependent inhibition of each of 4 SHH genes (*SHH*, *PTCH1*, *SMO*, and *GLI1*; Supplementary Figure 5C). There was good model convergence for *GLI1* and *SMO*. This suggests that there could be a minocycline target at or above the level of *SMO* or at *PTCH1* in canonical SHH signaling [40].

To confirm these RNA sequencing findings at the level of protein abundance, we measured concentrations of *PTCH1* (Figure 6), *GLI1* (Figure 7), and *SMO* (Supplementary Figure 6) in 12-well plates. Comparison of the effect of cyclopamine on *PTCH1*, the most potent inhibitor of SHH pathway known, by ANOVA showed that minocycline reduced *PTCH1* concentrations relative to those in nontreated controls on days 3 and 28 ($P = .0004$) of treatment to the same extent as cyclopamine ($P = .1510$; Figure 6A and 6B). The inflection point in the dose response was at a 0.5-mg/L dose of minocycline, after which *PTCH1* concentrations started to decrease ($r^2: 0.64–0.94$ for all days; Figure 6C). Figure 7 shows the effect of cyclopamine and minocycline on *GLI1*. Figure 7A shows time-dependent effects of treatments and the control on the transcriptional factor *GLI1*. In the first 14 days, minocycline decreased the concentration of *GLI1* to a level lower than that for nontreatment ($P = .0086$) and for cyclopamine ($P = .0004$); beyond 14 days, cyclopamine inhibition improved. On the other hand, there was no dose-dependent inhibition of *SMO* by minocycline, which is not surprising because SHH signaling occurs when *PTCH1* releases *SMO* from inhibition, rather than because of new *SMO* synthesis (Supplementary Figure 6). Overall, the results show that minocycline inhibited canonical SHH signaling at the same concentrations and potency as those associated with direct *M. tuberculosis* kill and MICs.

Determination of the Optimal Dose of Minocycline to Use in Patients With Tuberculosis in the Clinic

Finally, we performed a Monte Carlo experiment to identify the dose that would achieve the EC₈₀ in a 10 000-patient

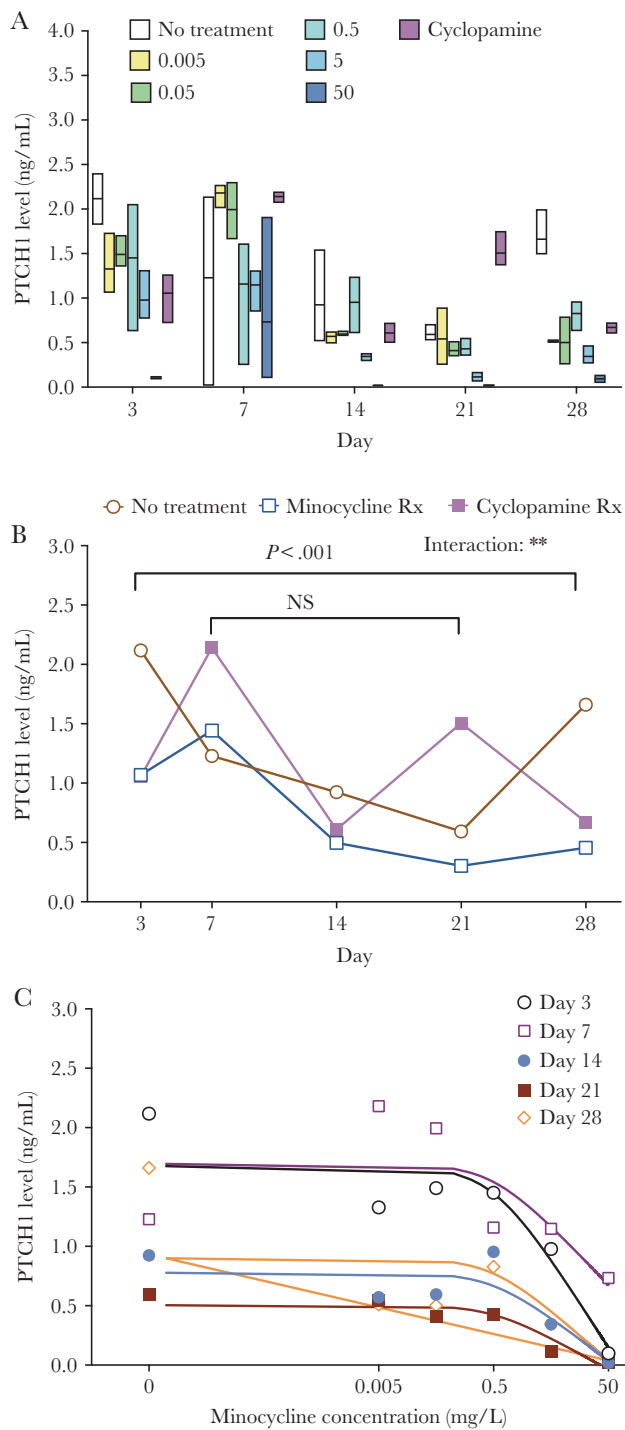


Figure 6. Effect of minocycline on protein patched homolog 1 (PTCH1). Enzyme-linked immunosorbent assay analysis of the sonic hedgehog (SHH) protein PTCH1 in adherent THP1 cells exposed to several concentrations of minocycline or 5 μ M of cyclophamide (positive control), in triplicate. *A*, Mean, minimum, and maximum concentrations of PTCH1. The effect of minocycline on PTCH concentrations was similar to that of cyclophamide, except on day 21. *B*, Results of repeated measures analysis of variance of all minocycline replicates combined, no treatment, and cyclophamide. Minocycline reduced PTCH1 concentrations relative to nontreated controls on days 3 and 28 ($P = .0004$) to the same extent as cyclophamide ($P = .1510$). *C*, Dose-response effect of the minocycline concentration on the PTCH1 concentration on days 3, 7, 14, 21, and 28. The inflection point in the dose response was at 0.5 mg/L minocycline, at which the PTCH concentration started to decrease (r^2 range, 0.64–0.94 for all days). NS, not significant.

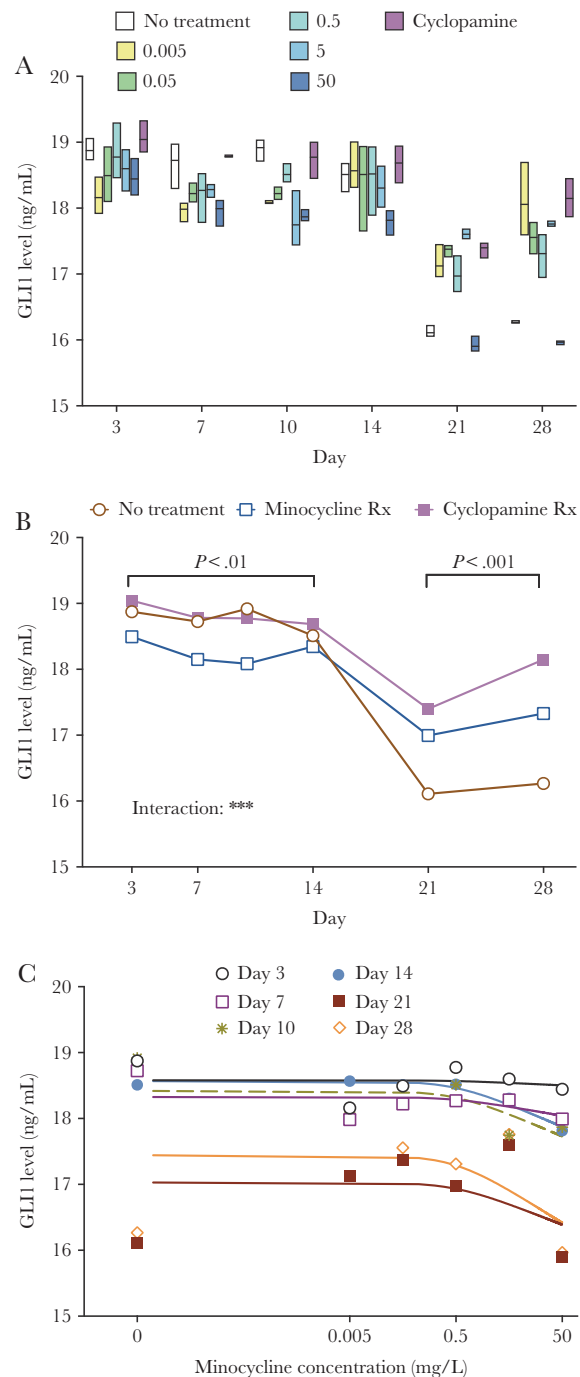


Figure 7. Minocycline effect on glioma-associated oncogene 1 (GLI1). Enzyme-linked immunosorbent assay results for the sonic hedgehog (SHH) protein GLI1 in adherent THP1 cells exposed to minocycline (several concentrations) or 5 μ M of cyclophamide (positive control), in triplicate. *A*, Mean, maximum, and minimum concentrations of GLI1. Minocycline had a time-dependent effect on the GLI1 concentration. Cyclophamide inhibited GLI1 in the latter half of the study period. *B*, Results of repeated measures analysis of variance of all minocycline replicates combined, no treatment, and cyclophamide. Minocycline yielded a lower concentration of GLI1 than cyclophamide until day 14, after which cyclophamide resulted in a greater GLI1 concentration. Thus, the treatment effect was time dependent ($P = .005$). In the first 14 days, minocycline decreased GLI1 concentrations, compared with the nontreated control ($P = .0086$) and cyclophamide ($P = .0004$). *C*, Dose-response effect of the minocycline concentration on the GLI1 concentration on different days. The dose response followed an umbrella pattern after day 14, with a peak at 0.05 mg/mL (r^2 range, 0.37–0.97).

population: the pharmacokinetic parameter output is shown in [Supplementary Table 1](#). Our simulation accurately recapitulated the input pharmacokinetic parameters and between-patient variability in the clinic ([Supplementary Table 1](#)). At doses of ≥ 5 mg/kg, target attainment was achieved in $>90\%$ of patients but was $<90\%$ at the MIC of 8 mg/L ([Supplementary Figure 7A](#)). This makes 8 mg/L the susceptibility breakpoint above which minocycline fails to treat tuberculosis. Evaluation of the proportion of 10 000 patients with tuberculosis in whom the EC_{80} was achieved for each dose over the entire MIC range found that the optimal daily dose is 7 mg/kg ([Supplementary Figure 7B](#)). Thus, the optimal dose for a 50-kg patient would be about 400 mg/day, with rounding to the nearest 100-mg dose owing to the size of the tablets in use.

DISCUSSION

SHH inhibition by cyclopamine after accidental ingestion by pregnant sheep resulted in lambs with craniofacial deformities and cyclopia [41, 42]. This is because SHH signaling is fundamental to morphogenesis, patterning, ECM generation, and cell polarity in utero. SHH plays the same role throughout life as part of tissue regeneration, healing, and fibrosis. We found that minocycline is a specific inhibitor of SHH signaling, likely at the level of PTCH1. Minocycline is considerably safer than cyclopamine and its derivatives and could be important in modulating lung remodeling in patients with tuberculosis. Upregulation of SHH signaling signatures, resulting in suppression of Toll-like receptor 2 responses, has been demonstrated in vitro and in patients with tuberculosis [43]. Furthermore, SHH interacts with a profibrotic, TGF- β , and with MMPs during chronic lung inflammation: the balance of these factors is associated with aberrant lung healing and fibrosis [35–39, 44]. Tuberculosis lung damage, volume loss, and fibrosis are due to excessive proteolytic ECM destruction, inefficient tissue remodeling, and vascular inflammatory responses [10]. These outcomes lead to severe physical impairment, poor quality of life, and premature death, despite adequate antibiotic therapy [10]. Indeed, posttuberculosis lung remodeling is arguably the most common cause of pulmonary fibrosis and chronic lung disability globally. However, to date, there has been no targeted therapy to mitigate tissue damage during either the early or late phase of tuberculosis. We also found that minocycline reduced transcript levels of *COL9A2* and *COL1A1*, which encode proteins associated with fibrotic lung response and ECM stiffening [32–34]. Minocycline could be used as targeted therapy to reduce lung, brain, and pericardial damage and fibrosis during tuberculosis. It will be important to follow up our in vitro findings with in vivo studies. To this end, given the similarity in SHH signaling between humans and other primates and the difference in signaling between humans and mice, we plan to test the minocycline in a macaque model of tuberculosis [45].

Second, some prior studies have shown that minocycline has antiapoptotic effects in microglia, whereas others have shown it to be proapoptotic in cancer cells [46, 47]. In addition, once *M. tuberculosis* has infected human cells, it engineers the captive cell to avoid apoptosis, thus ensuring bacterial survival. This escape mechanism also likely hides *M. tuberculosis* during both latent and active infection. We found that minocycline led to a level of *M. tuberculosis* killing sufficient to decrease the *M. tuberculosis* burden, effectively counteracting bacterial anti-apoptotic effect. Thus, minocycline is a bona fide host-directed therapy that also indirectly kills *M. tuberculosis*. In theory, the proapoptotic mechanism of minocycline would not be affected by development of acquired minocycline resistance by the bacilli. Thus, minocycline could be a novel therapy for latent infection, active infection due to drug-susceptible or MDR *M. tuberculosis*, and even infection due to minocycline-resistant *M. tuberculosis*.

According to World Health Organization guidelines, therapy for MDR-TB entails the use of at least 5 antibiotics (and often ≥ 7) for either 9–12 months or about 20 months. For XDR-TB, a cocktail of up to 8 drugs is administered for up to 24 months [10]. These regimens are associated with severe adverse events in 40%–70% of patients [9, 48, 49]. This contrasts with the rate of adverse events due to minocycline: for >15 million minocycline prescriptions, the rate was only 72 adverse events per million prescriptions [50]. Our proposed minocycline dose of 7 mg/kg/day is within the range that has been tolerated by patients in 2 prior stroke studies, but we plan to further examine the safety of the same dose in macaque tuberculosis studies [16, 17]. Moreover, the microbial kill rates of most second-line drugs are poor and are lower than those of first-line antituberculosis drugs. This results in a longer therapy duration. In contrast, minocycline had a microbial kill rate equal to or greater than that of first-line drugs. Thus, replacement of several second-line drugs by minocycline could potentially shorten the treatment duration for MDR-TB and XDR-TB. We found that 94% of 30 MDR-TB or XDR-TB clinical isolates were susceptible to minocycline at clinically achievable concentrations, which suggests that widespread susceptibility to minocycline is likely. Furthermore, minocycline has oral formulations, in contrast to aminoglycosides, costs only a few pennies, and is available worldwide, which could dramatically lower the cost of treatment for MDR-TB and XDR-TB in resource-constrained settings.

Finally, the minocycline concentration inside infected monocytes lagged behind extracellular pharmacokinetics, and the drug lingered longer, a phenomenon known as system hysteresis. Hysteresis occurs when effect lags behind its cause; that is, when the output value (ie, the intracellular concentration) is dependent on the history of input (ie, the extracellular concentrations) but lags in time. This suggests that minocycline could also exhibit hysteresis in other immune cells, leading to prolonged immunomodulation. In addition, the microbial effect could continue to be felt by intracellular *M. tuberculosis* long

after serum and lung tissue concentrations have declined below the MIC. This could be exploited for intermittent therapy and for treatment of latent *M. tuberculosis* infection.

In summary, minocycline has efficacy against both drug-susceptible and drug-resistant strains of *M. tuberculosis*. Second, it kills *M. tuberculosis* indirectly, via apoptosis, a mechanism likely to be important in treatment of both active and latent *M. tuberculosis* infection. Third, minocycline could also limit host lung damage by tuberculosis, based on its effect on inflammation, tissue remodeling, and SHH.

Supplementary Data

Supplementary materials are available at *The Journal of Infectious Diseases* online. Consisting of data provided by the authors to benefit the reader, the posted materials are not copyedited and are the sole responsibility of the authors, so questions or comments should be addressed to the corresponding author.

Notes

Acknowledgments. D. D. and T. G. were responsible for study conceptualization and methods and for the first draft of the manuscript. D. D., S. S., K. R. M., M. C., T. K., and P. S. L. were responsible for hollow fiber experiments. T. K. and S. S. were responsible for RNA sequencing and Western blots. J. G. P. and S. S. were responsible for bioinformatics analyses. T. G. was responsible for PK/PD modeling and simulations. K. D. was responsible for manuscript writing, with special emphasis on clinical translation. T. G., D. D., and K. D. were responsible for manuscript writing, with an emphasis on reviewing and editing. T. G. was responsible for funding acquisition and study supervision.

Meeting presentations. None

Financial support. This work was supported by the Baylor Research Institute.

Potential conflicts of interest. All authors: No reported conflicts. All authors have submitted the ICMJE Form for Disclosure of Potential Conflicts of Interest. Conflicts that the editors consider relevant to the content of the manuscript have been disclosed.

References

1. Duggar BM. Aureomycin; a product of the continuing search for new antibiotics. *Ann N Y Acad Sci* **1948**; 51:177–81.
2. Steenken W Jr, Wolinsky E. The tuberculostatic action of terramycin in vitro and in the experimental animal. *Ann N Y Acad Sci* **1950**; 53:309–18.
3. Steenken W Jr, Wolinsky E. Tuberculostatic activity of aureomycin in vitro and in vivo. *Am Rev Tuberc* **1949**; 59:221.
4. Pines A. Tetracycline in tuberculosis. *Br Med J* **1964**; 1:311.
5. Frisk AR, Tunevall G. Clinical evaluation of minocycline. *Antimicrob Agents Chemother (Bethesda)* **1968**; 8:335–9.
6. Walker NF, Clark SO, Oni T, et al. Doxycycline and HIV infection suppress tuberculosis-induced matrix metalloproteinases. *Am J Respir Crit Care Med* **2012**; 185:989–97.
7. Alsaad N, Wilffert B, van Altena R, et al. Potential antimicrobial agents for the treatment of multidrug-resistant tuberculosis. *Eur Respir J* **2014**; 43:884–97.
8. Gonzalo X, Casali N, Broda A, Pardiou C, Drobniewski F. Combination of amikacin and doxycycline against multidrug-resistant and extensively drug-resistant tuberculosis. *Int J Antimicrob Agents* **2015**; 45:406–12.
9. Dheda K, Limberis JD, Pietersen E, et al. Outcomes, infectiousness, and transmission dynamics of patients with extensively drug-resistant tuberculosis and home-discharged patients with programmatically incurable tuberculosis: a prospective cohort study. *Lancet Respir Med* **2017**; 5:269–81.
10. Dheda K, Gumbo T, Maartens G, et al. The epidemiology, pathogenesis, transmission, diagnosis, and management of multidrug-resistant, extensively drug-resistant, and incurable tuberculosis. *Lancet Respir Med* **2017**; 5:291–360.
11. Deshpande D, Srivastava S, Bendet P, et al. Antibacterial and sterilizing effect of benzylpenicillin in tuberculosis. *Antimicrob Agents Chemother* **2018**; 62:e02232–17.
12. Deshpande D, Srivastava S, Chapagain M, et al. Ceftazidime-avibactam has potent sterilizing activity against highly drug-resistant tuberculosis. *Sci Adv* **2017**; 3:e1701102.
13. Agwuh KN, MacGowan A. Pharmacokinetics and pharmacodynamics of the tetracyclines including glycylicyclines. *J Antimicrob Chemother* **2006**; 58:256–65.
14. Naline E, Sanceaume M, Toty L, Bakdach H, Pays M, Advenier C. Penetration of minocycline into lung tissues. *Br J Clin Pharmacol* **1991**; 32:402–4.
15. Saivin S, Houin G. Clinical pharmacokinetics of doxycycline and minocycline. *Clin Pharmacokinet* **1988**; 15:355–66.
16. Fagan SC, Waller JL, Nichols FT, et al. Minocycline to improve neurologic outcome in stroke (MINOS): a dose-finding study. *Stroke* **2010**; 41:2283–7.
17. Fouda AY, Newsome AS, Spellicy S, et al. Minocycline in acute cerebral hemorrhage: an early phase randomized trial. *Stroke* **2017**; 48:2885–7.
18. Metz LM, Li DKB, Traboulsee AL, et al.; Minocycline in MS Study Team. Trial of minocycline in a clinically isolated syndrome of multiple sclerosis. *N Engl J Med* **2017**; 376:2122–33.
19. Szeto GL, Pomerantz JL, Graham DR, Clements JE. Minocycline suppresses activation of nuclear factor of activated T cells 1 (NFAT1) in human CD4+ T cells. *J Biol Chem* **2011**; 286:11275–82.
20. Zink MC, Uhrlaub J, DeWitt J, et al. Neuroprotective and anti-human immunodeficiency virus activity of minocycline. *JAMA* **2005**; 293:2003–11.
21. Alffenaar JW, Gumbo T, Aarnoutse RE. Acquired drug resistance: we can do more than we think! *Clin Infect Dis* **2015**; 60:969–70.

22. Gumbo T, Pasipanodya JG, Romero K, Hanna D, Nuermberger E. Forecasting accuracy of the hollow fiber model of tuberculosis for clinical therapeutic outcomes. *Clin Infect Dis* **2015**; 61(Suppl 1):S25–31.
23. Chilukuri D, McMaster O, Bergman K, Colangelo P, Snow K, Toerner JG. The hollow fiber system model in the non-clinical evaluation of antituberculosis drug regimens. *Clin Infect Dis* **2015**; 61(Suppl 1):S32–3.
24. Deshpande D, Srivastava S, Pasipanodya JG, et al. Linezolid for infants and toddlers with disseminated tuberculosis: first steps. *Clin Infect Dis* **2016**; 63:80–7.
25. Deshpande D, Srivastava S, Nuermberger E, Pasipanodya JG, Swaminathan S, Gumbo T. Concentration-dependent synergy and antagonism of linezolid and moxifloxacin in the treatment of childhood tuberculosis: the dynamic duo. *Clin Infect Dis* **2016**; 63:88–94.
26. Srivastava S, Pasipanodya JG, Ramachandran G, et al. A Long-term co-perfused disseminated tuberculosis-3D liver hollow fiber model for both drug efficacy and hepatotoxicity in babies. *EBioMedicine* **2016**; 6:126–38.
27. Gumbo T, Louie A, Deziel MR, Parsons LM, Salfinger M, Drusano GL. Selection of a moxifloxacin dose that suppresses drug resistance in *Mycobacterium tuberculosis*, by use of an in vitro pharmacodynamic infection model and mathematical modeling. *J Infect Dis* **2004**; 190:1642–51.
28. Gumbo T, Angulo-Barturen I, Ferrer-Bazaga S. Pharmacokinetic-pharmacodynamic and dose-response relationships of antituberculosis drugs: recommendations and standards for industry and academia. *J Infect Dis* **2015**; 211(Suppl 3):S96–S106.
29. Srivastava S, Magombedze G, Koeuth T, et al. Linezolid dose that maximizes sterilizing effect while minimizing toxicity and resistance emergence for tuberculosis. *Antimicrob Agents Chemother* **2017**; 61:e00751-17.
30. Yamamoto T, Takano K, Matsuyama N, et al. Pharmacokinetic characteristics of minocycline in debilitated elderly patients. *Am J Ther* **1999**; 6:157–60.
31. Lieberman J. Granzyme A activates another way to die. *Immunol Rev* **2010**; 235:93–104.
32. Gimenez A, Duch P, Puig M, Gabasa M, Xaubet A, Alcaraz J. Dysregulated collagen homeostasis by matrix stiffening and TGF-beta1 in fibroblasts from idiopathic pulmonary fibrosis patients: role of FAK/Akt. *Int J Mol Sci* **2017**; 18:2431.
33. Marquis JF, Lacourse R, Ryan L, North RJ, Gros P. Genetic and functional characterization of the mouse Trl3 locus in defense against tuberculosis. *J Immunol* **2009**; 182:3757–67.
34. Bollong MJ, Yang B, Vergani N, et al. Small molecule-mediated inhibition of myofibroblast transdifferentiation for the treatment of fibrosis. *Proc Natl Acad Sci U S A* **2017**; 114:4679–84.
35. Daley WP, Peters SB, Larsen M. Extracellular matrix dynamics in development and regenerative medicine. *J Cell Sci* **2008**; 121:255–64.
36. Fitch PM, Howie SE, Wallace WA. Oxidative damage and TGF-a differentially induce lung epithelial cell sonic hedgehog and tenascin-C expression: implications for the regulation of lung remodelling in idiopathic interstitial lung disease. *Int J Exp Pathol* **2011**; 92:8–17.
37. Kugler MC, Joyner AL, Loomis CA, Munger JS. Sonic hedgehog signaling in the lung. From development to disease. *Am J Respir Cell Mol Biol* **2015**; 52:1–13.
38. Piera-Velazquez S, Mendoza FA, Jimenez SA. Endothelial to mesenchymal transition (EndoMT) in the pathogenesis of human fibrotic diseases. *J Clin Med* **2016**; 5.
39. Stewart GA, Hoyne GF, Ahmad SA, et al. Expression of the developmental Sonic hedgehog (Shh) signalling pathway is up-regulated in chronic lung fibrosis and the Shh receptor patched 1 is present in circulating T lymphocytes. *J Pathol* **2003**; 199(4):488–95.
40. Brennan D, Chen X, Cheng L, Mahoney M, Riobo NA. Noncanonical Hedgehog signaling. *Vitam Horm* **2012**; 88:55–72.
41. Binns W, James LF, Shupe JL. Toxicosis of veratrum californicum in ewes and its relationship to a congenital deformity in lambs. *Ann N Y Acad Sci* **1964**; 111:571–6.
42. Keeler RE, Binns W. Teratogenic compounds of *Veratrum californicum* (Durand). V. Comparison of cyclopien effects of steroidal alkaloids from the plant and structurally related compounds from other sources. *Teratology* **1968**; 1:5–10.
43. Ghorpade DS, Holla S, Kaveri SV, Bayry J, Patil SA, Balaji KN. Sonic hedgehog-dependent induction of microRNA 31 and microRNA 150 regulates *Mycobacterium bovis* BCG-driven toll-like receptor 2 signaling. *Mol Cell Biol* **2013**; 33:543–56.
44. Wallace WA, Fitch PM, Simpson AJ, Howie SE. Inflammation-associated remodelling and fibrosis in the lung - a process and an end point. *Int J Exp Pathol* **2007**; 88:103–10.
45. Dorus S, Anderson JR, Vallender EJ, et al. Sonic Hedgehog, a key development gene, experienced intensified molecular evolution in primates. *Hum Mol Genet* **2006**; 15:2031–7.
46. Ruiz-Moreno C, Velez-Pardo C, Jimenez-Del-Rio M. Minocycline induces apoptosis in acute lymphoblastic leukemia Jurkat cells. *Toxicol In Vitro* **2018**; 50:336–46.
47. Tikka T, Usenius T, Tenhunen M, Keinänen R, Koistinaho J. Tetracycline derivatives and ceftriaxone, a cephalosporin antibiotic, protect neurons against apoptosis induced by ionizing radiation. *J Neurochem* **2001**; 78:1409–14.
48. Modongo C, Sobota RS, Kesenoglu B, et al. Successful MDR-TB treatment regimens including amikacin are associated with high rates of hearing loss. *BMC Infect Dis* **2014**; 14:542.
49. Sotgiu G, Centis R, D'Ambrosio L, et al. Efficacy, safety and tolerability of linezolid containing regimens in treating MDR-TB and XDR-TB: systematic review and meta-analysis. *Eur Respir J* **2012**; 40:1430–42.
50. Smith K, Leyden JJ. Safety of doxycycline and minocycline: a systematic review. *Clin Ther* **2005**; 27:1329–42.